The kernel function $\sigma_{22}^{p}(X,\Xi)$ can be obtained by modifying Mindlin's solutions (Mindlin, 1936) for nuclei of strain in a semi-infinite space. For example, normal stress $\sigma_{22}^{3}(X,\Xi)$ caused by a point force in x_3-direction is as follows;

$$\begin{aligned}\sigma_{22}^{3} = \Bigg[& \frac{(1-2\nu)(-\xi_3+x_3)}{R_1^3} - \frac{3(\xi_2-x_2)^2(-\xi_3+x_3)}{R_1^5} \\ & + \frac{(1-2\nu)[3(-\xi_3+x_3)-4\nu(-\xi_3-x_3)}{R_2^3} \\ & - \frac{3(3-4\nu)(\xi_2-x_2)^2(-\xi_3+x_3)-6z(\xi_3+x_3)\,[(1-2\nu)(-\xi_3)-2\nu(-x_3)]}{R_2^5} \\ & - \frac{30(-x_3)(\xi_2-x_2)^2\xi_3(-\xi_3+x_3)}{R_2^7} \\ & - \frac{4(1-\nu)(1-2\nu)}{R_2(R_2-\xi_3-x_3)}\left(1-\frac{(\xi_2-x_2)^2}{R_2(R_2-\xi_3-x_3)}-\frac{(\xi_2-x_2)^2}{R_2^2}\right)\Bigg] \end{aligned} \tag{2}$$

where $X = X(x_1\,,\ x_2,\ x_3)$ and $\Xi = \Xi(\xi_1\,,\ \xi_2,\ \xi_3)$, and R_1 and R_2 are given by;

$$R_1 = [(\xi_1-x_1)^2+(\xi_2-x_2)^2+(\xi_3-x_3)^2]^{1/2} \tag{3}$$

$$R_2 = [(\xi_1-x_1)^2+(\xi_2-x_2)^2+(\xi_3+x_3)^2]^{1/2} \tag{4}$$

NUMERICAL FORMULATION

It is quite cumbersome to obtain analytical solutions to the integral equation (1). In this work, instead, we employ a numerical integration with a MATLAB code. As a first step, the surface of the crack is digitized by a finite element mesh (Figure 3a). Standard elements in the finite element mesh are 8-node elements whereas the elements located at the crack tip (hereafter crack tip element) have 9 nodes (Li et al., 1998). Each node in X-coordinate system (Figure 3a) on an element is mapped onto a master element in ζ-coordinate system with 9 (=3×3) Gauss points (Figure 3b).

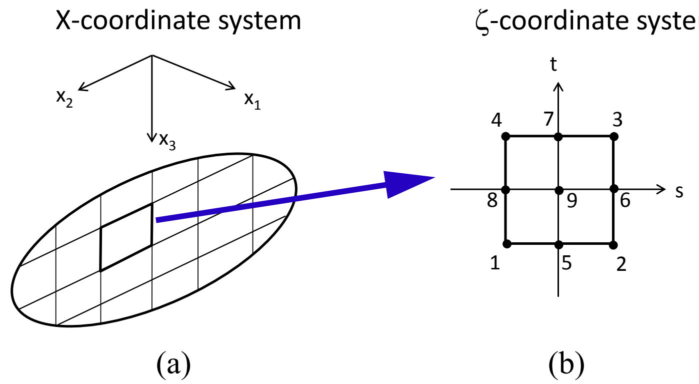

Figure 3, Mapping of (a) nodes on a finite element on the crack surface in *X*-coordinate system onto (b) a master element in ζ-coordinate system.

The numerical integration is conducted by the Gaussian quadrature (e.g., Bhatti, 2005). Standard elements use standard interpolation functions, h_i for 8-node standard elements (e.g., Bathe, 2006) whereas crack tip elements uses interpolation functions, h_i', as follows (Li et al., 1998);

$$h_i(s,t) = \frac{\sqrt{1+\pi}}{A_i} h_i'(s,t) \tag{5}$$

where i is the node number (Figure 3b), h_i' are interpolation functions for a 9-node standard element, and

$$A_i = \begin{cases} \sqrt{1+t} & for\ t \neq -1 \\ \dfrac{1}{2} & for\ t = -1 \end{cases} \tag{6}$$

In this way, the coordinate interpolations using isoparametric formulation are;

$$x_1 = \sum_{i=1}^{n} h_i(s,t) x_1^i \tag{7}$$

$$x_2 = \sum_{i=1}^{n} h_i(s,t) x_2^i \tag{8}$$

$$x_3 = \sum_{i=1}^{n} h_i(s,t) x_3^i \tag{9}$$

where x_j^i are the x_j coordinates (j = 1, 2, and 3) at node i and n is the total number of nodes in each element; i.e., n = 8 for standard elements and n = 9 for crack tip elements. Furthermore, tangent vector can be expressed as

$$J_s = (\frac{\partial x_1}{\partial s}, \frac{\partial x_2}{\partial s}, \frac{\partial x_3}{\partial s}) \tag{10}$$

$$J_t = (\frac{\partial x_1}{\partial t}, \frac{\partial x_2}{\partial t}, \frac{\partial x_3}{\partial t}) \tag{11}$$

and, Jacobian, $\det J$, is determined as

$$\det J = |J_s \times J_t| \tag{12}$$

Then, with Gaussian quadrature, numerical integration of a function, $f(x_1, x_2, x_3)$, can be expressed as (e.g., Bathe, 2006):

$$\int_{-1}^{1}\int_{-1}^{1} f\big(x_1(s,t), x_2(s,t), x_3(s,t)\big) \det J ds dt = \sum_{i,j}^{m} w_i w_j\, f(r_i, s_j) \tag{13}$$

where $\det J$ is the Jacobian, m is the number of Gauss points, and, $w_{i,}$ are corresponding weights. In this work, the function f in equation (5) represents $\sigma_{11}^{p}(X, \Xi)\Delta u(\Xi)$ inside the integral in equation (1). By adding contribution of the crack opening at each node on the crack surface to the displacement at an arbitrary point in the semi-finite solid, displacement at the point due to the crack can be calculated.

In addition to the consideration of the impact of the surface of the semi-infinite solid (Figure 1), this method has an advantage over analytical solutions that the only input data for the crack morphology in equation (1) is the crack opening at each node and its coordinates. Therefore, all the nodes do not have to be located on a single plane and complicated morphology of a pressurized crack such as non-planar, non-elliptic crack can be accommodated.

RESULTS OF MODELING

In this section, we present the modeling results of two cases; Cases 1 and 2 to validate our code. In both cases, a penny-shaped crack is located inside a semi-infinite elastic solid and it is a planar crack with crack opening, $\Delta u(\Xi)$ specified at a point, $\Xi(\xi_1,\ \xi_2,\ \xi_3)$ on the crack surface of which radius is a and its center is located at (0, 0, c) (Figures 1 and 2) as follows

$$u(\Xi) = \Delta u_{max}\sqrt{1 - \left(\frac{\xi_1}{a}\right)^2 - \left(\frac{\xi_3 - c}{a}\right)^2} \tag{14}$$

where Δu_{max} is the maximum crack opening at its center.

In Case 1, the center of a penny-shaped crack with radius of 1.0 m and maximum opening of 1 cm is located at depth of 1000 m. Figure 4 shows the u_3 distribution along x_2-direction (x_1 = 0.0) at depths of 900 m (i.e., close to the crack), 500 m (i.e., at an intermediate distance from the crack), and 0 m (i.e., on the surface of the semi-infinite solid), and these results are compared with those from Fabrikant's (1989) solutions. Since Fabrikant's solutions are for an infinite medium, for example, displacement from Fabrikant's solutions at depth 900 m in Figure 4 actually means the displacement at a distance of 100 m (=1000 m – 900 m) from the center of the crack in x_3-direction. At depth of 900 m, difference between u_3 from our code and that from the Fabrikant's solutions is negligible (Figure 4a) At shallower depths (or, at a greater distance from the crack), the difference is getting conspicuous (Figures 4b and 4c). These results indicate that our code produces the same results as analytical solutions do at a close distance from the crack. However, as the distance from the crack increases, there is a noticeable difference between them. This difference comes from the lack of consideration of the surface of the semi-infinite solid. In other words, the Fabrikant's solutions underestimate displacement by ignoring the lack of constraint at the surface whereas there is no obvious difference between both approaches (i.e. the analytical method and our numerical method) at points close to the crack where the impact of the surface is negligible.

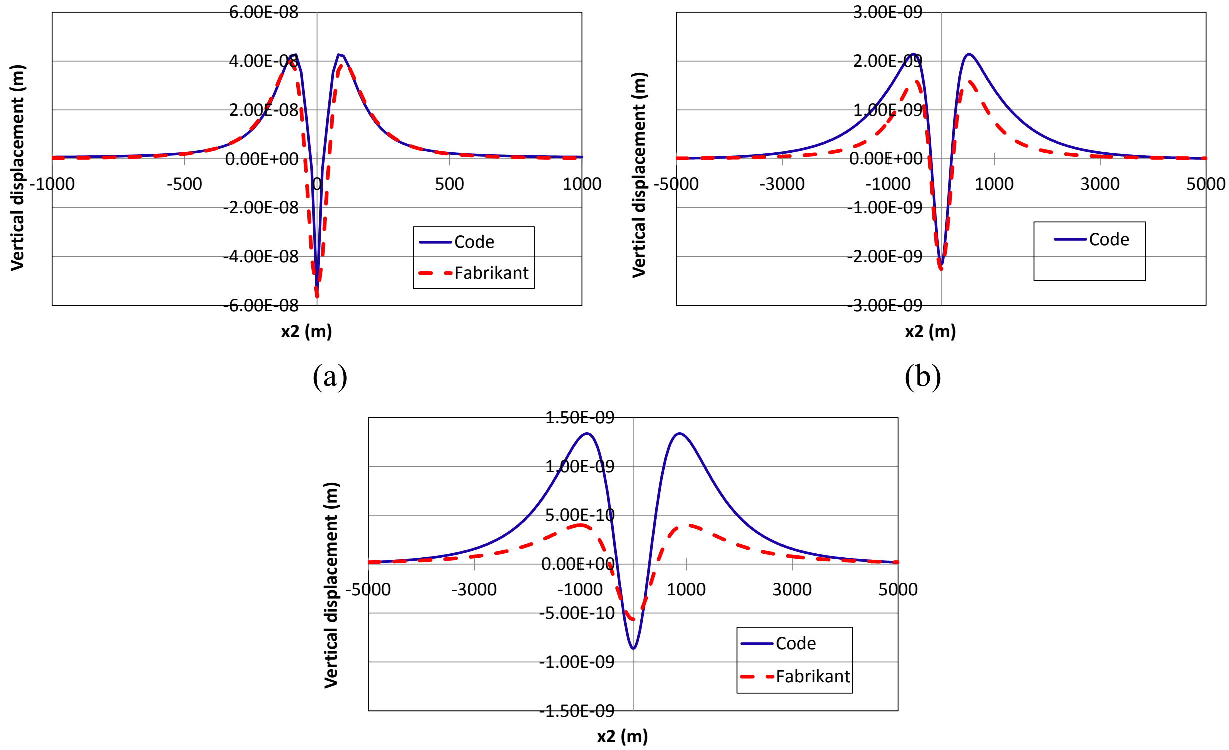

(a) (b)

(c)

Figure 4, Comparison of vertical displacement (u_3) distribution along x_2-axis (x_1 = 0.0) at depths of (a) 900 m (b) 500 m, and (c) 0 m (surface) where "Code" and "Fabrikant" denote results from our code and Fabrikant's (1989) solutions, respectively. For the convenience of interpretation, upward vertical displacement is considered positive here in contrast to the coordinate system in Figure 1.

Case 2 models the deformation of a semi-infinite medium in which the center of a penny-shaped crack with diameter 2 m and maximum opening 1 cm is located at a depth of 20 m (Figure 1). Vertical displacement u_3 distribution along x_2 direction (x_1 = 0.0) at depth of 0.0 m (i.e., on the surface) from both approaches are compared in Figure 5. As expected, our code provides significantly greater displacement than Fabrikant's solutions do. This result suggests that analytical solutions for infinite medium may significantly underestimate ground deformation, which may lead to damage to pre-existing structures if analytical solutions are employed to predict ground surface deformation. On the other hand, Figure 6 presents the vertical displacement (u_3) distribution on a plane at depth of 0.0 m and surface deformation predicted by our code is in a good agreement with previous researches (e.g. Wright et al., 1996).

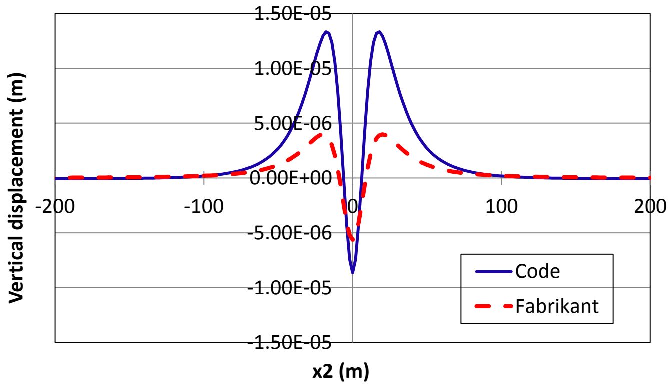

Figure 5, Comparison of vertical displacement (u_3) distribution along x_2-axis (x_1 = 0.0) at depth of 0.0 m.

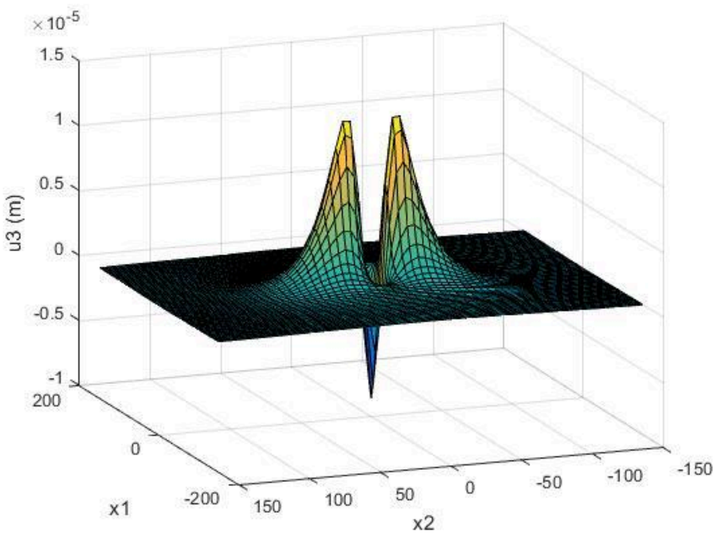

Figure 6, Vertical displacement (u_3) distribution on a plane at depth of 0.0 m.

CONCLUSIONS

A numerical code has been developed for modeling of surface deformation due to a pressurized crack with complex morphology in a semi-infinite elastic solid using MATLAB. Somigliana's formula is modified for a governing equation and the normal stresses of Mindlin's solutions for nuclei of strain in a semi-infinite solid are employed as kernel functions. The governing equation in the form of an integral equation is solved with Gaussian quadrature. This code has advantages over conventional analytical solutions that it can accommodate complex morphology of a non-planar crack with arbitrary shape.

The performance of the code is evaluated by comparing the results from the code with those from analytical solutions for a penny-shaped crack under uniform pressure in an infinite solid. This comparison suggests that this code can produce the sufficiently close results at points near the crack to that from analytical solutions where the impact of the surface of the semi-infinite solid is negligible, validating the code. Furthermore, it was observed that the difference between the two approaches is increasing as the point at which deformations are evaluated with the two methods. This result indicates that analytical solutions may significantly underestimate the ground deformation produced by hydraulic fracturing due to the lack of consideration of the ground surface, and a new approach such as our numerical method that is able to take into account the impact of the ground surface is required. It is also shown that our method can provide better prediction of ground surface deformation than the analytical methods do.

Acknowledgements

The authors are especially thankful to Drs. Marko E. Mear and Gregory J. Rodin in the Department of Aerospace Engineering and Engineering Mechanics at the University of Texas at Austin for the original idea about the numerical formulation.

References

Adams, J. and Rowe, C. (2013). “Differentiating Applications of Hydraulic Fracturing.” Chapter 18 in *Effective and Sustainable Hydraulic Fracturing,* Bunger, A.P., McLennan, J and Jeffrey, R., eds. INTECH, Rijeka, Croatia, 391-400.

Bathe, K. J. (2006). *Finite Element Procedures*, Prentice-Hall International, NJ.

Bhatti, M. A. (2005). “*Fundamental finite element analysis and applications.*” John Wiley & Sons, Hoboken, NJ, 381-466.

Davis, P. M. (1983). “Surface deformation associated with a dipping hydrofracture.” *J. of Geophys. Res.: Solid Earth*, 88(B7), 5826-5834.

Fabrikant, V. I. (1989). “Applications of Potential Theory in Mechanics: A Selection of New Results.” *J. Appl. Mech.*, 60(3), 71-79.

Feng, Y. J., and Shi, X. W. (2013). “Hydraulic fracturing process: roles of in situ stress and rock strength.” *Adv. Mat. Res.,* Trans Tech Publications, 616, 435-440.

Green, A. E. and Sneddon, I. N. (1950). “The distribution of stress in the neighbourhood of a flat elliptical crack in an elastic solid.” *Math. Proc. Cambridge Philos. Soc.*, Cambridge University Press, 46(1), 159-163.

Li, S., Mear, M.E., and Xiao, L. (1998) Symmetric weak-form integral equation method for three-dimensional fracture analysis, *Computer Methods in Applied Mechanics and Engineering*, 151(3–4), 435-459.

Love, A. E. H. (2013). *A Treatise on the Mathematical Theory of Elasticity.* Cambridge university press, England.

MathWorks (2017) *MATLAB Documentation*, https://www.mathworks.com/help/matlab/

Mindlin, R. D. (1936). “Force at a point in the interior of a semi-infinite solid.” *J. Appl. Phys.*, 7(5), 195-202.

Okada, Y. (1992) “Internal Deformation due to Shear and Tensile Faults in a Half-Space.” *Bull. Seismol. Soc. Am.*, 82(2), 1018-1040.

Pollard, D. D., and Holzhausen, G. (1979). “On the mechanical interaction between a fluid-filled fracture and the Earth's surface.” *Tectonophysics*, 53(1-2), 27-57.

Rongved, L. and Frasier, J. T. (1958). “Displacement Discontinuity in the Elastic Half Space.” *J. Appl. Mech.*, 25,125-128.

Rummel, F. and Kappelmayer, O. (1983). “The Falkenberg Geothermal Frac Project: Concepts and Experimental Results.” In: *Hydraulic fracturing and geothermal energy,* Nemat-Nasser, S., Abé, H., and Hirakawa, S., eds. Hydraulic Fracturing and Geothermal Energy, 59-74.

Rungamornrat, J., Wheeler, M.F., and Mear, M.E. (2005). “Coupling of fracture/non-newtonian flow for simulating nonplanar evolution of hydraulic fractures”, *Proceedings of SPE Annual Technical Conference and Exhibition*, 9-12 October, 2005, Dallas, Texas, SPE-96968-MS

Sun, R. J. (1969). “Theoretical Size of Hydraulically Induced Horizontal Fractures and Corresponding Surface Uplift in an Idealized Medium.” *J. Geophys. Res.*, 74(25) 5995-6011.

Valkó, P., and Economides, M. J. (1995). *Hydraulic fracture mechanics* (Vol. 318). Chichester: Wiley.

Warpinski, N. R. (2000). “Analytic crack solutions for tilt fields around hydraulic fractures.” *J. Geophys. Res.: Solid Earth*, *105*(B10), 23463-23478.

Williamson, W. H. and Woolley, D. R. (1980). *Hydraulic fracturing to improve the yield of bores in fractured rock.* Australian Government Publishing Service.

Wright, C.A., Davis, E.J., Minner, W.A., Ward, J.F., Weijers, L., Schell, E.J., and Hunter, S.P. (1998). “Surface tiltmeter fracture mapping reaches new depths - 10,000 feet and beyond.” *Proceedings of Society of Petroleum Engineers Rocky Mountain Regional/Low-Permeability Reservoirs Symposium*, 5-8 April, Denver, Colorado, SPE-39919-MS.

Influence of Mesh Size, Number of Slices, and Number of Simulations in Probabilistic Analysis of Slopes Considering 2D Spatial Variability of Soil Properties

Brigid Cami[1]; Sina Javankhoshdel, Ph.D.[2]; Richard J. Bathurst, Ph.D.[3]; and Thamer Yacoub, Ph.D.[4]

[1]Rocscience Inc., 54 Saint Patrick St., Toronto, ON, Canada M5T 1V1. E-mail: brigid.cami@rocscience.com
[2]Rocscience Inc., 54 Saint Patrick St., Toronto, ON, Canada M5T 1V1. E-mail: sina.javankhoshdel@rocscience.com
[3]GeoEngineering Centre at Queen's-RMC, Dept. of Civil Engineering, Royal Military College of Canada, 13 General Crerar, Kingston, ON, Canada K7K 7B4. E-mail: bathurst-r@rmc.ca
[4]Rocscience Inc., 54 Saint Patrick St., Toronto, ON, Canada M5T 1V1. E-mail: thamer.yacoub@rocscience.com

Abstract

The random limit equilibrium method (RLEM) is a relatively new method of probabilistic slope stability analysis which uses a combination of 2D random field theory, limit equilibrium methods, and Monte Carlo simulation. The random finite element method (RFEM) uses a combination of 2D random field theory, finite element method of analysis, strength reduction method, and Monte Carlo simulation. In this paper, the effects of mesh size, number of slices, and number of Monte Carlo simulations on computed probability of failure are investigated using both approaches. Computation times using both methods to solve the same slope problem are also compared. Recommendations for mesh size, number of slices, and number of Monte Carlo simulations, with respect to the spatial correlation length, using RLEM are presented.

INTRODUCTION

Two methods of probabilistic slope stability analysis which consider 2D spatial variability are examined in this study: the non-circular Random Limit Equilibrium Method (RLEM), and the Random Finite Element Method (RFEM). The RLEM is a relatively new method of probabilistic slope stability analysis which uses a combination of 2D random field theory, circular or non-circular limit equilibrium methods and Monte Carlo simulation. RFEM uses a combination of 2D random field theory, finite element method of analysis, strength reduction method, and Monte Carlo simulation. Two disadvantages of the RFEM method are the large computational effort required, and convergence problems for the case of slopes with very small mesh size. The purpose of this paper is to examine the effect of mesh size, number of slices, and number of Monte Carlo simulations (MC) on computed probability of failure (PF) using RLEM analysis, and to compare the results using RFEM.

RFEM. Griffiths et al. (2009) applied the RFEM to undrained cohesive and cohesive-frictional soil slopes. A random field of each shear strength parameter (cohesion and friction angle) was generated using the local average subdivision method (LAS) developed by Fenton and Vanmarcke (1990) and then mapped onto the finite element mesh. The elements are assigned different values of each soil property, but elements close to each other are correlated using horizontal and vertical correlation lengths (Θ). Theoretically, the correlation structures of the underlying Gaussian random field can be determined using the Markov correlation coefficient function:

$$R\left(\tau_x, \tau_y\right)=\exp\left\{-\sqrt{\left(\frac{2\tau_x}{\theta_x}\right)^2+\left(\frac{2\tau_y}{\theta_y}\right)^2}\right\} \quad [1]$$

where, $R(\tau_x, \tau_y)$ is the autocorrelation coefficient, τ_x and τ_y are the absolute distances between two points in horizontal and vertical directions, respectively. θ_x and θ_y are the spatial correlation lengths in horizontal and vertical directions, respectively. For the isotropic case where $\theta_x = \theta_y = \theta$, Equation 1 can be simplified to:

$$R\left(\tau\right)=\exp\left\{-\frac{2\tau}{\theta}\right\} \quad [2]$$

where τ is the absolute distance between two points in the isotropic field. In the remainder of the paper, the spatial correlation length is normalized to the height of the slope (H).

In this study, the open-source FEM code (mrslope2d) by Fenton and Griffiths (2008) was used to carry out the RFEM analyses.

RLEM. Probabilistic stability analyses results considering spatial variability of soil properties and using LEM have been reported in studies by Li and Lumb (1987), El-Ramly et al. (2001), Low (2003), Babu and Mukesh (2004), Cho (2007 and 2010), Tabbaroki et al. (2013), Li et al. (2014), Javankhoshdel and Bathurst (2014) and Javankhoshdel et al. (2017).

Javankhoshdel et al. (2017) used a circular slip limit equilibrium method and random field theory to investigate the influence of spatial variability of soil properties on probability of failure. Tabbaroki et al. (2013) used a non-circular limit equilibrium approach together with random field theory to consider spatial variability in their probabilistic analyses.

In the RLEM, a random field is first generated using the local average subdivision (LAS) method and then mapped onto a grid mesh, similar to the FEM mesh in RFEM analyses. Each mesh element in the random field has different values of soil properties, and cells close to one another have values that are different in magnitude, based on the value of the spatial correlation length. In each realization, a search is carried out to find the mesh elements intersected by the slip surface. Random soil property values are assigned to all slices whose base mid-point falls within that element. A limit equilibrium approach is then used to calculate factor of safety (FS) for each realization. The probability of failure is calculated as the ratio of the number of simulations resulting in FS < 1 to the total number of simulations.

Non-Circular RLEM

The non-circular RLEM used in this study is a combination of a refined search and the LEM approach (Morgenstern-Price method). The refined search is based on circular surfaces that are converted to piece-wise linear surfaces. The search for the lowest factor of safety is refined as the search progresses. An iterative approach is used so that the results of one iteration are used to narrow the search area for the most critical slope failure mechanism in the next iteration.

The refined search in this study was used together with an additional optimization technique. The optimization is based on a Monte Carlo technique, often referred to as "random walking" (Greco 1996). When used in conjunction with a non-circular search, this optimization method can be very effective at locating (searching out) slip surfaces with lower factors of safety.

In this study, a version of the program *Slide* v.8, which is currently in development (Rocscience Inc. 2017) was used to carry out the non-circular RLEM analyses.

The Slope Model. A simple 27 degree slope with a slope height of 10 m and a foundation depth of 10 m was used for the purpose of this study. The slope geometry and problem domain are shown in Figure 1. The Morgenstern-Price limit equilibrium method was used with the half sine interslice force function to calculate factor of safety.

Cohesion (c) and friction angle (ϕ) were considered to be random variables with typical coefficients of variation (COV) of 0.5 and 0.2, respectively. The mean values of these parameters were taken as: c = 5 kPa; ϕ = 20 degrees; unit weight (γ) = 20 kN/m^3. Lognormal distributions were assumed for all random variables. Only isotropic spatial variability is considered in this paper. ($\Theta_x = \Theta_y$).

Ching and Phoon (2012), Huang and Griffiths (2015), and Ching and Hu (2016) investigated the effect of mesh size used in finite element models that include soil properties with spatial variability. However, similar sensitivity analyses using non-circular RLEM have not been undertaken prior to this paper.